ACS APPLIED ENERGY MATERIALS

www.acsaem.org Letter

Assessing Utilization Boundaries for Pt-Based Catalysts in an Operating Proton-Exchange Membrane Fuel Cell

Michal Ronovsky, Lujin Pan, Malte Klingenhof, Isaac Martens, Lukas Fusek, Peter Kus, Raphael Chattot, Marta Mirolo, Fabio Dionigi, Harriet Burdett, Jonathan Sharman, Peter Strasser, Alex Martinez Bonastre, and Jakub Drnec*

Cite This: *ACS Appl. Energy Mater.* 2023, 6, 8660−8665 Read Online

ACCESS | Metrics & More | Article Recommendations | Supporting Information

ABSTRACT: Octahedra (oh) PtNiX/C catalysts are notable cathode catalysts for proton-exchange membrane fuel cells due to their exceptional oxygen reduction reaction activity. Here, we investigate the degradation of oh-PtNiIr catalysts under fuel-cell conditions using operando X-ray diffraction (XRD). Employing two accelerated stress tests with different lower potential limits and XRD-coupled cyclic voltammetry on benchmark Pt and oh-PtNiIr catalysts, we find that dissolution and degradation are proportional to the extent of reduction, independent of the catalyst's nature. Our method identifies the optimal potential range for Pt-based catalysts to minimize degradation without lengthy stress tests.

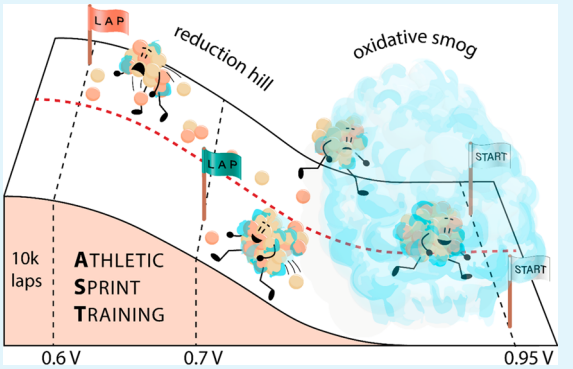

KEYWORDS: *PEMFC catalyst, degradation, voltage control, dissolution by reduction, operando X-ray diffraction, octahedra, Pt alloys*

The need for a hydrogen economy is becoming integral to transitioning to a carbon-neutral future, as we try to reduce our carbon footprint. Given the critical role of noble metals for oxygen reduction reaction (ORR) catalysis, much research has been dedicated to improving the catalytic activity of Pt by modifying its electronic and structural properties via Pt alloying with transition metals (Co, Ni, and Fe).[1,2] In 2007, Stamenkovic et al. identified the most active surface, $Pt_3Ni(111)$, which led to the development of PtNi octahedral nanoparticles (NPs) with 10-fold mass- and area-specific activity gain in the rotating disk electrode (RDE) configuration due to maximization of the surface availability of PtNi(111) facets.[1,3,4] However, transferring the activity measured in RDE experiments to a proton-exchange membrane fuel cell (PEMFC) and reaching stability targets remains a significant challenge for many of the highly active PtNi binary and ternary catalysts in the shape of nanoframes and octahedra.[4]

Several challenges remain in transposing the phenomenal activity and durability reported in wet electrochemical cells of alloy catalysts to real devices. Octahedra (oh) NPs (5−8 nm) have a smaller electrochemical surface area (ECSA) than commercial 2−3 nm Pt catalysts, but at the same time, the rate constant for the ORR is at least 10 times higher than that of Pt. Thus, octahedra must accommodate and withstand a larger current per NP at a constant loading to produce the same overall current at a given voltage. As a result of the higher turnover frequency for the ORR, (oh) alloy NPs have higher water concentration in the vicinity of the catalyst. This can lead to local oxygen starvation due to the inhibited oxygen diffusion to the NP surface. In addition, accommodating increased current density (per NP) requires a well-structured boundary that allows not only sufficient oxygen diffusion but also good proton and electron conductivity.[5]

Besides the problems described above, withstanding potential changes during PEMFC operation is perhaps the biggest challenge because the dissolution of Ni or Pt degrades the finely tuned structure of oh-PtNi catalysts and thus lowers the catalytic activity. One way to stabilize the structure is to dope oh-PtNi with a small amount of additional metal such as Ir, Mo, or Rh.[6−8] While this is a promising improvement and the stability objectives are reached in the RDE configuration, performance in the membrane electrode assembly (MEA) configurations that meet the stability target following the Department of Energy testing protocol has not been reported yet.

It is agreed that the stability is linked to the extent of platinum oxide growth and reduction, which leads to various

Received: May 17, 2023
Accepted: August 28, 2023
Published: August 31, 2023

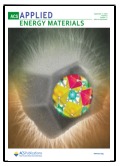

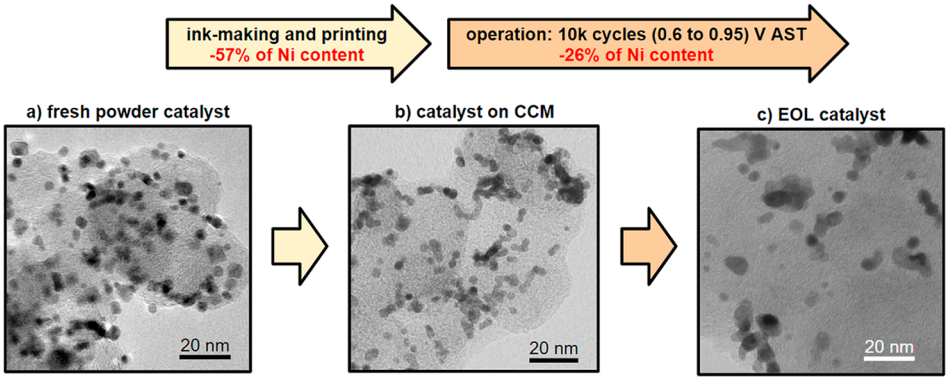

Figure 1. TEM images of the oh-PtNiIr catalyst at three stages: (a) as-prepared powder; (b) as-prepared CCM; (c) EOL catalyst after 10K cycles of 0.6−0.95 V AST. The ink-making/printing procedure leached out 57% of the Ni content and made the edges of the octahedra less pronounced. The AST leached out only 26% of the Ni content but caused severe structural degradation.

degrees of dissolution and degradation. Up until now, much research has focused on the Pt oxidation−dissolution link. Many publications highlighted the influence of the upper potential limit (UPL) in an accelerated stress test (AST), making clear that increasing the UPL increases the extent of oxidation and, in turn, the extent of dissolution.[9−11] However, only a limited amount of research focused on the influence of the lower potential limit (LPL).[12−14] By conducting a thorough flow-cell experiment, Đukić et al. illustrated the importance of controlling the LPL to improve the PEMFC catalyst's lifetime, which they attributed to the reduction kinetics of surface oxides,[15] but direct physical evidence is missing, and the actual mechanism between the LPL and the stability of the catalyst in MEAs remains unknown. This is critical for the field because meeting the catalysts' activity and durability targets will enable large-scale commercial adoption of PEMFCs and the hydrogen economy.

In this work, we explore the dissolution mechanics of a PtNiIr/C octahedral catalyst (doped with <1 atom % Ir) and compare it with a reference commercial Pt/C catalyst. With a focus on the LPL and reduction potentials, we investigate the linkage between the catalyst degradation and operational boundaries in a 5 cm^2 PEMFC optimized for high-energy X-ray diffraction (XRD) measurement. The fast acquisition rate enabled by the high flux of EBS-ESRF allows tracking oxidation/reduction processes during the device operation with a high temporal resolution. We conclude that Pt and Ni dissolution is proportional not only to the extent of Pt oxidation but, interestingly, also to the extent of Pt reduction, which can depend on its kinetics.

For the experiments shown in this work, we use two types of catalyst-coated membranes (CCMs) prepared by Johnson Matthey (JM): (i) "Pt(JM)" benchmark CCM with Pt (the volume-weighted diameter is 2.9 nm, as determined using XRD) on both the cathode (0.187 mg_{Pt}/cm^2) and anode (0.079 mg_{Pt}/cm^2) that serves as the reference material; (ii) "oh-PtNiIr" CCM with octahedral-shaped (oh) PtNiIr (0.100 mg_{Pt}/cm^2 and 0.017 mg_{Ni}/cm^2; the volume-weighted diameter is 7.1 nm) at the cathode and Pt (0.079 mg_{Pt}/cm^2) at the anode. Loadings were measured at JM using X-ray fluorescence after spray-coating the Nafion112 membrane.

We find that the oh-PtNiIr catalyst incorporated in the CCM already has a different composition from the as-synthesized oh-PtNiIr powder: Energy-dispersive X-ray (EDX) analysis (Figure S7) shows that the oh-PtNiIr powder has an atomic Pt:Ni ratio of 2.20, whereas the as-prepared oh-PtNiIr CCM has a ratio of 6.35. This suggests that the catalyst lost 57% of its Ni atomic content during ink-making and printing. Such a high loss of a transition-metal alloying element has been observed and discussed previously in the work of Gatalo and Dubau.[16,17] It has been pointed out that the CCM-making process, together with the activation potential cycling, can alter the catalyst morphology and composition to such an extent that the catalyst is no longer the same material as was synthesized, questioning the common approaches to catalyst activity testing using the RDE technique.[18] Our results provide further evidence that this is also the case for multimetallic oh-PtNiIr.

In contrast to compositional changes, the structural changes are less noticeable in the ink-making/printing step [transmission electron microscopy (TEM) micrographs in Figure 1a,b]. Qualitatively, the edges of octahedral NPs are less pronounced in the catalyst coated on the membrane than in the catalyst powder, indicating that loss of the octahedral shape happened to some extent. Figure 1c shows the catalyst after 10K cycles of a standard 0.6−0.95 V AST. At the end of life (EOL), the atomic Pt:Ni ratio is 8.33, meaning 26% of the Ni atomic content leaches out. Thus, 2 times more Ni content dissolved during the ink-making/printing procedure compared to the AST. It is clear that serious attention must be focused on adapting the ink-making/printing procedure to retain the composition of state-of-the-art multimetallic catalysts during the MEA preparation. From Figure 1c, we can see that Ni dissolution itself is not the only degradation mechanism. NPs also aggregate, coalesce, and ripen, and carbon support corrodes.[19]

In laboratory conditions, catalyst degradation is typically studied by square-wave ASTs. The U.S. DRIVE Fuel Cell Technical Team adopted the standard of cycling from 0.6 to 0.95 V with a 3 s dwell time at both the LPL and UPL.[20] This test mimics the dynamics of the typical fuel-cell (FC) operation with Pt dissolution and Ostwald ripening as preferential degradation pathways.[9,21,22] Even though the mechanism of Pt degradation and dissolution as a function of the UPL is well-known,[12,23,24] the exact nature of the rather surprising linkage between the LPL and Pt degradation is still unclear.[12,13,15,16]

To study the effects of lower potentials on the aging of oh-PtNiIr and Pt(JM) catalysts, we perform two square-wave ASTs with different LPLs: 0.6−0.95 and 0.7−0.95 V,

https://doi.org/10.1021/acsaem.3c01243
ACS Appl. Energy Mater. 2023, 6, 8660−8665

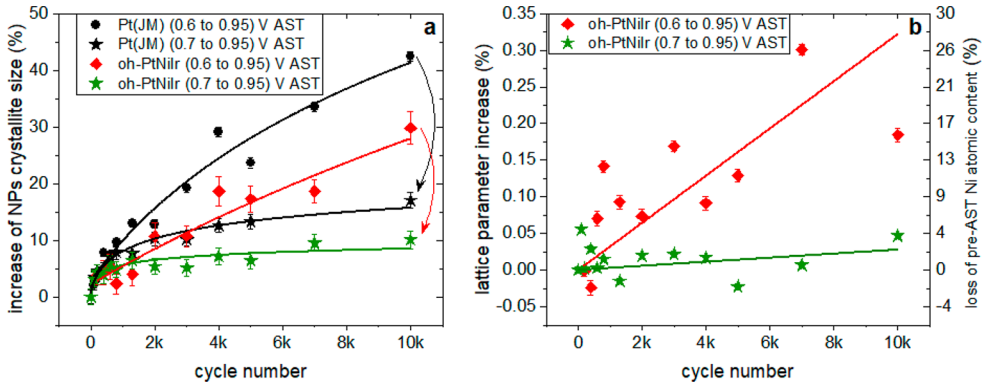

Figure 2. (a) Crystallite size evolution of Pt(JM) (black) and oh-PtNiIr (red/green) catalysts during 10K cycles of two square-wave ASTs. In the case of 0.6 V AST, the Pt(JM) size increase is 42% and that for oh-PtNiIr 30%, whereas in the case of 0.7 V AST, the Pt(JM) size increase is 17% and that for oh-PtNiIr 10%. The lines of the logarithmic function are provided to guide the reader through data points. (b) Lattice parameter evolution of oh-PtNiIr for 0.6 and 0.7 V AST. A linear function was used to approximate the loss of Ni atomic content. The error bars correspond to the Rietveld fit uncertainty.

hereinafter referred to as 0.6 V LPL and 0.7 V LPL ASTs, respectively. We use a custom-built 5 cm^2 FC operating at 80 °C, at 80% relative humidity, and flowing H_2/O_2 at 200 sccm.[25] Both Pt(JM) and oh-PtNiIr MEAs made from as-prepared CCMs with Sigracet 22BB gas diffusion layers were conditioned at constant current densities for approximately 2 h (Figure S3). The ECSA, specific activity, mass activity, and polarization curves are provided in Figure S5. Throughout the 10K cycles of each AST, we follow structural changes of the catalyst with XRD (Figure S6).[25] In general, we obtain three parameters from XRD analysis: scale factor, lattice parameter, and crystallite size.

(1) The scale factor, i.e., scattering intensity, corresponds to the total amount of scatterers. Thus, it can be used to track dissolution. Also, Martens et al. proposed that the scale factor decreases at oxidizing potentials due to the formation of an amorphous oxide layer on Pt NPs.[24] On time scales where the dissolution is negligible, the scale factor is thus a direct indicator of the amorphous oxide growth/reduction onset.

(2) The lattice parameter is a global measure of strain. In bimetallic systems, the changes can be caused by dissolution, following Vegard's law,[26] or by the evolution of surface tension due to the field effect and adsorption phenomena.[27] Changes in the lattice parameter manifest as shifts in the diffraction peak positions.

(3) The crystallite size is the size of the coherently scattering domain. The size of the scattering domain does not change during aggregation, but it changes during coalescence and ripening. Thus, depending on the degradation process, one NP can be composed of a few such domains.[28] Harsher degradation leads, in general, to a more pronounced crystallite size increase.

Figure 2a shows the evolution of the crystallite sizes of Pt(JM) and oh-PtNiIr throughout 10K cycles with different LPLs. The 0.6 V LPL AST is significantly harsher as the crystallite sizes of the NPs increase throughout 10K cycles by 42% for Pt(JM) and 30% for oh-PtNiIr, whereas in the case of the 0.7 V LPL AST, they increase by only 17% for Pt(JM) and 10% for oh-PtNiIr, respectively. The degradation and ripening of the NPs are the fastest at the beginning of the AST for both catalysts. In Figure 2b, we show the evolution of the lattice parameter of the oh-PtNiIr catalyst for 0.6 V LPL AST (diamonds) and 0.7 V LPL AST (stars). Ni dissolution is substantial in the case of 0.6 V LPL AST as the lattice parameter increases from 3.8835 ± 0.0016 to 3.8943 ± 0.0004 Å, corresponding to a (27 ± 2)% loss of the pre-AST Ni atomic content, which is well in line with the 26% loss of Ni measured by EDX. In contrast, in the case of 0.7 V LPL AST, Ni loss was only (3 ± 2)% from the pre-AST Ni atomic content. These observations agree with the previously reported dependence of dissolution on the LPL for Pt[12] and PtCo nanocatalysts.[16] Although the size increase for the oh-PtNiIr catalyst is still substantial even for 0.7 V LPL AST, its resistance to Ni dissolution is greatly improved. The positive effect of increasing the LPL on the degradation extent seems to be universal and independent of the catalyst's nature (particle size, composition, electrode loading, carbon support type, etc.), even though the details (potential limits and kinetics) will likely be different for each catalyst.

To build the connection between the LPL and dissolution mechanism, we follow cyclic voltammetry (CV) at 50 mV/s with XRD over several cycles (XRD-CV). The top part of Figure 3 shows the evolution of the scale factor (brown) for Pt(JM), while the bottom part shows the same for oh-PtNiIr. Because the first CV cycle is clearly different from subsequent ones due to impurity removal and reconstruction of the surface, only the second cycle is shown (Figure S4).[18] For more details about the measurement protocol, see the experimental section in the Supporting Information (SI).

As expected, the Pt−O reduction region in the CV profiles is shifted toward higher potentials for oh-PtNiIr compared to the Pt(JM) catalyst. This is a consequence of OH bond weakening, which is related to a d-band shift induced by alloying with a less noble metal. Similar to Stamenkovic's work on single crystals, we see a negative shift of the H_{upd} region for the oh-PtNiIr catalyst with associated extension in the potential range of the double-layer region with respect to Pt(JM).[1] However, assessing the actual reduction onsets just by CV is complicated due to the convolution of multiple electrochemical processes happening on the electrode's surface (adsorption and place exchange). XRD-CV offers significant perspicuity because the scale factor onset directly corresponds to the place exchange and the reversed process, causing degradation and dissolution.[24]

To unambiguously follow the growth of surface oxide, we start the anodic sweep at 0.05 V, where the catalyst is fully reduced (corresponding to a scattering intensity of 1 au). In general, the XRD scale factor follows the oxidation/reduction

https://doi.org/10.1021/acsaem.3c01243
ACS Appl. Energy Mater. 2023, 6, 8660−8665

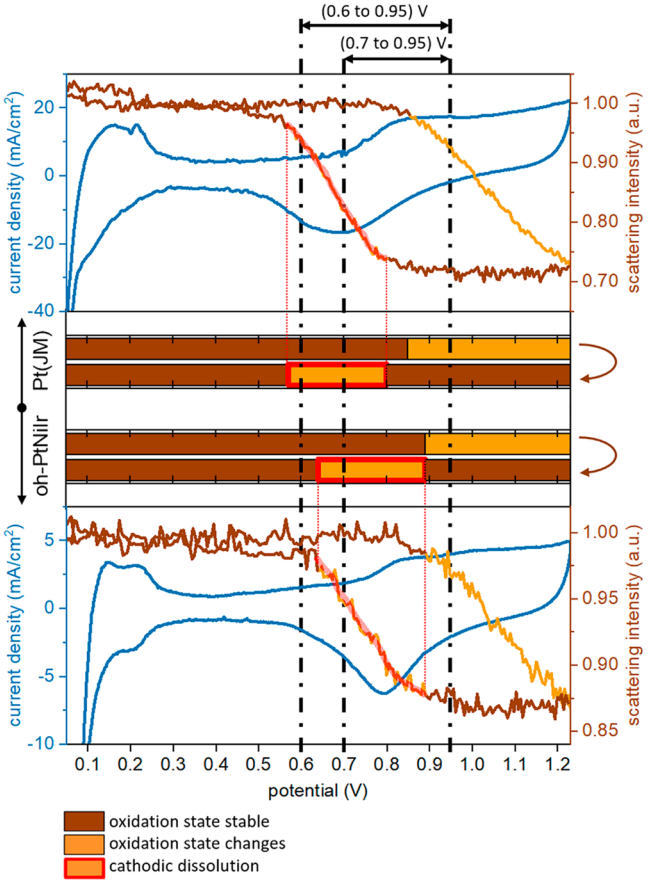

Figure 3. XRD was coupled with CV. The scale factor (brown) was obtained from XRD during CV with a 50 mV/s scan rate. The upper half shows the results from Pt(JM) and the lower part those from oh-PtNiIr. The cathodic dissolution region is highlighted by a red curve that extends into a simplified diagram, where the same region is highlighted by a red box. Black vertical dash-dotted lines mark the potential boundaries of two types of ASTs.

hysteresis apparent in CV. It is constant up to the onset of the oxidation potential, after which it decreases until a reverse potential of 1.23 V. At the beginning of the cathodic sweep, the scale factor rests at its lowest value and starts increasing when the potential crosses the onset of the reduction potential. After passing a reduction region (highlighted in red in Figure 3), the scale factor returns close to its original value, as Pt dissolution is negligible in such a short experiment time. There is a slight slope between the end of the reduction region and 0.05 V in the cathodic sweep, pointing to the fact that the catalyst is not yet entirely reduced. A small number of catalytic sites, presumably highly oxophilic defects, are much harder to reduce, giving rise to this slope.[29,30] Nevertheless, the reduction is ~97% complete at the end of the reduction region for both catalysts (Figure 3). Further, there is a slight difference between both the oxidation and reduction onsets for Pt(JM), but no difference is observed for oh-PtNiIr within the 0.02 V resolution limit. Note that, for the Pt catalyst, Martens et al. showed the dependence of the hysteresis width on a scan rate caused by slow reduction kinetics.[24] The oh-PtNiIr catalyst shows no scan rate dependence, confirming its fast redox kinetics (see Figures S1 and S2 for more details). The discussion of the influence of catalyst parameters, such as particle size, shape, carbon type, loading, etc., on the observed profiles is given in the SI. It is important to note that all of the parameters have an impact on the lifetime durability of the device. Nevertheless, the conclusion drawn from this work is that catalyst degradation is much more affected by the extent of Pt reduction in comparison to the particle size, shape, alloying, carbon type, etc.

Finally, we connect the degradation data from ASTs with the oxidation/reduction dynamics shown in XRD-CV. Setting the LPL to 0.6 V during AST results in a fully reduced oh-PtNiIr catalyst (the scattering intensity in XRD-CV reaches its fully reduced value), while at 0.7 V LPL, the reduction is only partial for both Pt(JM) and oh-PtNiIr. Given that the 0.7 V LPL AST results in much less degradation, the dissolution amount must be proportional to both the degree of oxidation and the degree of reduction, and it is independent of the catalyst's nature. This result also implies that the oxophilic sites that are more difficult to reduce (likely the uncoordinated sites) are stable in the oxide form but are prone to dissolution once reduced. Therefore, one of the strategies to limit the dissolution is to keep those vulnerable sites permanently oxidized, e.g., by altering their electronic structure by ternary/quaternary metal doping or increasing the LPL.

Such knowledge has a direct implication for the operation of a FC, especially for high-active shape-controlled Pt alloys. Their activity is strongly bound to a specific crystal structure, and the extent of surface restructuring during the reduction will affect this activity to a larger extent than those of other catalysts. In general, if we want to preserve high performance, we must carefully select the operational boundaries and limit both the lower and higher potential boundaries, regardless of the catalyst type. In the automotive industry, where multimetallic catalysts will be used to lower the stack's cost, the loss in power density at higher LPL can be compensated for by a more active catalyst and thus significantly higher current densities at lower overpotentials. Moreover, operating at higher LPLs increases the FC efficiency.

In conclusion, we have shown the practicality of the XRD-CV technique to explain the degradation behavior and provided further important insight into catalyst degradation mechanisms in an operational PEMFC. We have found specific onsets of a key crystallographic parameter (scale) associated with the oxidation, reduction, and degradation of two types of catalysts. By employing two ASTs with different LPLs (0.6–0.95 and 0.7–0.95 V), we showed a strong dependence of catalyst degradation on the LPL for oh-PtNiIr and confirmed this dependence for Pt/C.

Combining these two results, we conclude that the extent of degradation is proportional not only to the degree of oxidation but also to the degree of reduction within a cycle, independent of the catalyst's nature. While other approaches (e.g., tuning of the surface composition and electronic structure) to improve stability and retain activity are important and effective at the RDE level, they are not enough, and an operational boundary must be set on both lower and higher potential limits. Once the activity enhancement is transferred from a laboratory to the device, this approach will work best for automotive applications where a multimetallic catalyst reduces the stack's price, the increased exchange current density does not reduce the power density, and operation at higher voltages increases the FC efficiency. We think that limiting the LPL is a crucial step for implementing alloyed catalysts into PEMFCs and FC automotive as such. Moreover, the presented methodology can be further developed to serve as a benchmark measurement to

https://doi.org/10.1021/acsaem.3c01243
ACS Appl. Energy Mater. 2023, 6, 8660–8665

explore the operational boundaries for all kinds of Pt-based catalysts.

■ ASSOCIATED CONTENT

Supporting Information

The Supporting Information is available free of charge at https://pubs.acs.org/doi/10.1021/acsaem.3c01243.

oh-PtNiIr faster kinetics and microstrain, effect of catalyst parameters on the observed trends of scattering intensity and microstrain, experimental section, and raw data references (PDF)

■ AUTHOR INFORMATION

Corresponding Author

Jakub Drnec − *The European Synchrotron Radiation Facility (ESRF), 38000 Grenoble, France;* orcid.org/0000-0002-9520-1555; Email: drnec@esrf.fr

Authors

Michal Ronovsky − *The European Synchrotron Radiation Facility (ESRF), 38000 Grenoble, France;* orcid.org/0000-0002-8702-6056

Lujin Pan − *Electrochemical Energy, Catalysis and Material Science Laboratory, Department of Chemistry, Technical University Berlin, 10623 Berlin, Germany*

Malte Klingenhof − *Electrochemical Energy, Catalysis and Material Science Laboratory, Department of Chemistry, Technical University Berlin, 10623 Berlin, Germany*

Isaac Martens − *The European Synchrotron Radiation Facility (ESRF), 38000 Grenoble, France*

Lukas Fusek − *Faculty of Mathematics and Physics, Department of Surface and Plasma Science, Charles University, 18000 Prague 8, Czech Republic*

Peter Kus − *Faculty of Mathematics and Physics, Department of Surface and Plasma Science, Charles University, 18000 Prague 8, Czech Republic;* orcid.org/0000-0002-2246-4426

Raphael Chattot − *ICGM, Université Montpellier, CNRS, ENSCM, 34095 Montpellier Cedex 5, France;* orcid.org/0000-0001-6169-530X

Marta Mirolo − *The European Synchrotron Radiation Facility (ESRF), 38000 Grenoble, France;* orcid.org/0000-0002-6781-2762

Fabio Dionigi − *Electrochemical Energy, Catalysis and Material Science Laboratory, Department of Chemistry, Technical University Berlin, 10623 Berlin, Germany;* orcid.org/0000-0002-0576-024X

Harriet Burdett − *Johnson Matthey Technology Centre, Reading RG4 9NH, United Kingdom*

Jonathan Sharman − *Johnson Matthey Technology Centre, Reading RG4 9NH, United Kingdom*

Peter Strasser − *Electrochemical Energy, Catalysis and Material Science Laboratory, Department of Chemistry, Technical University Berlin, 10623 Berlin, Germany;* orcid.org/0000-0002-3884-436X

Alex Martinez Bonastre − *Johnson Matthey Technology Centre, Reading RG4 9NH, United Kingdom*

Complete contact information is available at: https://pubs.acs.org/10.1021/acsaem.3c01243

Author Contributions

The manuscript was written through contributions of all authors. All authors have given approval to the final version of the manuscript.

Notes

The authors declare no competing financial interest.

■ ACKNOWLEDGMENTS

Many thanks go to Alexandra Ronovska for her work on the graphical abstract. This project has received funding from the European Union's Horizon 2020 research and innovation program under the Marie Skłodowska-Curie Grant Agreement 847439. The GAIA project has received funding from the Fuel Cells and Hydrogen 2 Joint Undertaking (now Clean Hydrogen Partnership) under Grant Agreement 826097. This Joint Undertaking receives support from the European Union's Horizon 2020 research and innovation program, Hydrogen Europe, and Hydrogen Europe Research. This project has received funding from the Clean Hydrogen Partnership under Grant Agreement 101101346. This Joint Undertaking receives support from the European Union's Horizon 2020 Research and Innovation program, Hydrogen Europe, and Hydrogen Europe Research and is funded by the European Union under Grant 10110149. Views and opinions expressed are, however, those of the author(s) only and do not necessarily reflect those of the European Union. Neither the European Union nor the Clean Hydrogen Joint Undertaking can be held responsible for them.

■ REFERENCES

(1) Stamenkovic, V. R.; Fowler, B.; Mun, B. S.; Wang, G.; Ross, P. N.; Lucas, C. A.; Marković, N. M. Improved Oxygen Reduction Activity on $Pt_3Ni(111)$ via Increased Surface Site Availability. *Science* **2007**, *315* (5811), 493−497.

(2) Zhang, C.; Shen, X.; Pan, Y.; Peng, Z. A Review of Pt-Based Electrocatalysts for Oxygen Reduction Reaction. *Front. Energy Power Eng. Chin.* **2017**, *11* (3), 268−285.

(3) Huang, X.; Zhao, Z.; Cao, L.; Chen, Y.; Zhu, E.; Lin, Z.; Li, M.; Yan, A.; Zettl, A.; Wang, Y. M.; Duan, X.; Mueller, T.; Huang, Y. Electrochemistry. High-Performance Transition Metal-Doped Pt_3Ni Octahedra for Oxygen Reduction Reaction. *Science* **2015**, *348* (6240), 1230−1234.

(4) Pan, L.; Ott, S.; Dionigi, F.; Strasser, P. Current Challenges Related to the Deployment of Shape-Controlled Pt Alloy Oxygen Reduction Reaction Nanocatalysts into Low Pt-Loaded Cathode Layers of Proton Exchange Membrane Fuel Cells. *Curr. Opin. Electrochem.* **2019**, *18*, 61−71.

(5) Kongkanand, A.; Mathias, M. F. The Priority and Challenge of High-Power Performance of Low-Platinum Proton-Exchange Membrane Fuel Cells. *J. Phys. Chem. Lett.* **2016**, *7* (7), 1127−1137.

(6) Lin, R.; Che, L.; Shen, D.; Cai, X. High Durability of Pt-Ni-Ir/C Ternary Catalyst of PEMFC by Stepwise Reduction Synthesis. *Electrochim. Acta* **2020**, *330*, No. 135251.

(7) Dionigi, F.; Weber, C. C.; Primbs, M.; Gocyla, M.; Bonastre, A. M.; Spöri, C.; Schmies, H.; Hornberger, E.; Kühl, S.; Drnec, J.; Heggen, M.; Sharman, J.; Dunin-Borkowski, R. E.; Strasser, P. Controlling Near-Surface Ni Composition in Octahedral PtNi(Mo) Nanoparticles by Mo Doping for a Highly Active Oxygen Reduction Reaction Catalyst. *Nano Lett.* **2019**, *19* (10), 6876−6885.

(8) Beermann, V.; Gocyla, M.; Willinger, E.; Rudi, S.; Heggen, M.; Dunin-Borkowski, R. E.; Willinger, M.-G.; Strasser, P. Rh-Doped Pt-Ni Octahedral Nanoparticles: Understanding the Correlation between Elemental Distribution, Oxygen Reduction Reaction, and Shape Stability. *Nano Lett.* **2016**, *16* (3), 1719−1725.

(9) Cherevko, S.; Keeley, G. P.; Geiger, S.; Zeradjanin, A. R.; Hodnik, N.; Kulyk, N.; Mayrhofer, K. J. J. Dissolution of Platinum in

the Operational Range of Fuel Cells. *ChemElectroChem.* **2015**, *2* (10), 1471−1478.
(10) Myers, D. J.; Wang, X.; Smith, M. C.; More, K. L. Potentiostatic and Potential Cycling Dissolution of Polycrystalline Platinum and Platinum Nano-Particle Fuel Cell Catalysts. *J. Electrochem. Soc.* **2018**, *165* (6), F3178−F3190.
(11) Wang, X.; Kumar, R.; Myers, D. J. Effect of Voltage on Platinum Dissolution. *Electrochem. Solid State Letters* **2006**, *9* (5), A225.
(12) Zhang, H.; Haas, H.; Hu, J.; Kundu, S.; Davis, M.; Chuy, C. The Impact of Potential Cycling on PEMFC Durability. *J. Electrochem. Soc.* **2013**, *160* (8), F840−F847.
(13) Uchimura, M.; Sugawara, S.; Suzuki, Y.; Zhang, J.; Kocha, S. S. Electrocatalyst Durability under Simulated Automotive Drive Cycles. In *ECS Transactions*; ECS, 2008. DOI: 10.1149/1.2981858.
(14) Maselj, N.; Gatalo, M.; Ruiz-Zepeda, F.; Kregar, A.; Jovanovič, P.; Hodnik, N.; Gaberšček, M. The Importance of Temperature and Potential Window in Stability Evaluation of Supported Pt-Based Oxygen Reduction Reaction Electrocatalysts in Thin Film Rotating Disc Electrode Setup. *J. Electrochem. Soc.* **2020**, *167* (11), No. 114506.
(15) Đukić, T.; Moriau, L. J.; Pavko, L.; Kostelec, M.; Prokop, M.; Ruiz-Zepeda, F.; Šala, M.; Dražić, G.; Gatalo, M.; Hodnik, N. Understanding the Crucial Significance of the Temperature and Potential Window on the Stability of Carbon Supported Pt-Alloy Nanoparticles as Oxygen Reduction Reaction Electrocatalysts. *ACS Catal.* **2022**, *12* (1), 101−115.
(16) Gatalo, M.; Bonastre, A. M.; Moriau, L. J.; Burdett, H.; Ruiz-Zepeda, F.; Hughes, E.; Hodgkinson, A.; Šala, M.; Pavko, L.; Bele, M.; Hodnik, N.; Sharman, J.; Gaberšček, M. Importance of Chemical Activation and the Effect of Low Operation Voltage on the Performance of Pt-Alloy Fuel Cell Electrocatalysts. *ACS Appl. Energy Mater.* **2022**, *5* (7), 8862−8877.
(17) Dubau, L.; Asset, T.; Chattot, R.; Bonnaud, C.; Vanpeene, V.; Nelayah, J.; Maillard, F. Tuning the Performance and the Stability of Porous Hollow PtNi/C Nanostructures for the Oxygen Reduction Reaction. *ACS Catal.* **2015**, *5* (9), 5333−5341.
(18) Chattot, R.; Roiron, C.; Kumar, K.; Martin, V.; Campos Roldan, C. A.; Mirolo, M.; Martens, I.; Castanheira, L.; Viola, A.; Bacabe, R.; Cavaliere, S.; Blanchard, P.-Y.; Dubau, L.; Maillard, F.; Drnec, J. Break-In Bad: On the Conditioning of Fuel Cell Nanoalloy Catalysts. *ACS Catal.* **2022**, *12*, 15675−15685.
(19) Okonkwo, P. C.; Ige, O. O.; Barhoumi, E. M.; Uzoma, P. C.; Emori, W.; Benamor, A.; Abdullah, A. M. Platinum Degradation Mechanisms in Proton Exchange Membrane Fuel Cell (PEMFC) System: A Review. *Int. J. Hydrogen Energy* **2021**, *46* (29), 15850−15865.
(20) Perry, R. L. Analysis of Durability of MEAs in Automotive PEMFC Applications. 2012. https://www.hydrogen.energy.gov/pdfs/review12/fc089_perry_2012_o.pdf (accessed 2023-04-17).
(21) Topalov, A. A.; Cherevko, S.; Zeradjanin, A. R.; Meier, J. C.; Katsounaros, I.; Mayrhofer, K. J. J. Towards a Comprehensive Understanding of Platinum Dissolution in Acidic Media. *Chem. Sci.* **2014**, *5* (2), 631−638.
(22) Ehelebe, K.; Knöppel, J.; Bierling, M.; Mayerhöfer, B.; Böhm, T.; Kulyk, N.; Thiele, S.; Mayrhofer, K. J. J.; Cherevko, S. Platinum Dissolution in Realistic Fuel Cell Catalyst Layers. *Angew. Chem., Int. Ed. Engl.* **2021**, *60* (16), 8882−8888.
(23) Khedekar, K.; Rezaei Talarposhti, M.; Besli, M. M.; Kuppan, S.; Perego, A.; Chen, Y.; Metzger, M.; Stewart, S.; Atanassov, P.; Tamura, N.; Craig, N.; Cheng, L.; Johnston, C. M.; Zenyuk, I. V. Probing Heterogeneous Degradation of Catalyst in PEM Fuel Cells under Realistic Automotive Conditions with Multi-modal Techniques. *Adv. Energy Mater.* **2021**, *11* (35), No. 2101794.
(24) Martens, I.; Chattot, R.; Rasola, M.; Blanco, M. V.; Honkimäki, V.; Bizzotto, D.; Wilkinson, D. P.; Drnec, J. Probing the Dynamics of Platinum Surface Oxides in Fuel Cell Catalyst Layers Using in Situ X-Ray Diffraction. *ACS Appl. Energy Mater.* **2019**, *2* (11), 7772−7780.
(25) Martens, I.; Vamvakeros, A.; Chattot, R.; Blanco, M. V.; Rasola, M.; Pusa, J.; Jacques, S. D. M.; Bizzotto, D.; Wilkinson, D. P.; Ruffmann, B.; Heidemann, S.; Honkimäki, V.; Drnec, J. X-Ray Transparent Proton-Exchange Membrane Fuel Cell Design for in Situ Wide and Small Angle Scattering Tomography. *J. Power Sources* **2019**, *437*, No. 226906.
(26) Vegard, L. Die Konstitution der Mischkristalle und die Raumfüllung der Atome. *Z. Phys.* **1921**, *5* (1), 17−26.
(27) Chattot, R.; Martens, I.; Mirolo, M.; Ronovsky, M.; Russello, F.; Isern, H.; Braesch, G.; Hornberger, E.; Strasser, P.; Sibert, E.; Chatenet, M.; Honkimäki, V.; Drnec, J. Electrochemical Strain Dynamics in Noble Metal Nanocatalysts. *J. Am. Chem. Soc.* **2021**, *143* (41), 17068−17078.
(28) Martens, I.; Chattot, R.; Drnec, J. Decoupling Catalyst Aggregation, Ripening, and Coalescence Processes inside Operating Fuel Cells. *J. Power Sources* **2022**, *521*, No. 230851.
(29) Janik, M. J.; McCrum, I. T.; Koper, M. T. M. On the Presence of Surface Bound Hydroxyl Species on Polycrystalline Pt Electrodes in the "hydrogen Potential Region" (0−0.4 V-RHE). *J. Catal.* **2018**, *367*, 332−337.
(30) Chattot, R.; Bordet, P.; Martens, I.; Drnec, J.; Dubau, L.; Maillard, F. Building Practical Descriptors for Defect Engineering of Electrocatalytic Materials. *ACS Catal.* **2020**, *10* (16), 9046−9056.

https://doi.org/10.1021/acsaem.3c01243
ACS Appl. Energy Mater. 2023, 6, 8660−8665